A Multiscale Parametrization for Refractivity Estimation in the Troposphere

Uygar Karabaş*,†, Youssef Diouane*, Rémi Douvenot†,
*ISAE-SUPAERO, Université de Toulouse, 31400 Toulouse, France.
†ENAC, TELECOM, Université de Toulouse, 31400 Toulouse, France.
uygar.karabas@enac.fr

***Abstract*—This paper presents the idea of multiscale parametrization for tropospheric refractivity inversion using gradient-based optimization method. Our motivation is to improve the accuracy of inversion without the use of apriori information. We retrieve the details of the refractivity distribution progressively from large to smaller scales using hierarchical multiscale strategies in the admissible parameter space. The proposed formulation for multiscale adjoint tomography is validated and is confronted to a numerical test. This study shows that such strategies can potentially resolve complex ducting conditions which would otherwise fail a plain gradient-based inversion.**

***Index Terms*—Inverse Problems; Troposphere Propagation; Multiscale Adjoint Method.**

I. Introduction

Radar coverage in maritime environment depends on ambient refractive index in the lower troposphere. Non-standard refractivity variations may create anomalous propagation conditions which diminish performance of seaborne surveillance platforms. In order to provide the platform with real-time situational awareness about radar coverage, Refractivity-From-Clutter (RFC) is proposed [1]. The goal of RFC is to invert ambient refractivity from sea surface radar clutter [2].

The inverse problem is driven by the simulations of Parabolic Wave Equation (PWE). Initial RFC techniques have required lots of PWE simulations, so their scope has been limited to the problems with small parameter dimension [3]. Since the work in [4], high-dimensional RFC problems are solved efficiently using the adjoint state method. The last decade has seen progress in the development of adjoint-based RFC techniques (e.g., [5]) commonly relying on regularization.

The inversion of refractive index in PWE is a complex nonlinear ill-posed problem. The mitigation of nonlinearity and ill-posedness is searched by guessing what the missing information about the problem might be so that the solutions become physical. Accordingly, regularization and space reduction techniques have been used in RFC systems. Their advantage is that many non-physical local minima can be avoided during gradient-based optimization iterations. However, one may not always have quality apriori information to choose the regularization technique and construct the reduction basis.

Instead, we are interested in exploring the advantages of using Multiscale Parametrization Techniques (MPT) in RFC. We are motivated by the contribution of multiscale strategies in recent progress in acoustic full-waveform inverse problem in geophysics (e.g., [6]). In this paper, we apply the multiscale strategy in the parametrization, being inspired from the ideas in [7]. As an intermediate step towards RFC, we work on the 2-D tomography problem which is illustrated in Fig. 1, as in [4]. This choice is firstly due to that there is still work in progress for both RFC and tomography problems even in 2-D configuration. Secondly, the tomography problem is less complex problem than RFC, so analyzing it can help us develop real-time accurate RFC systems.

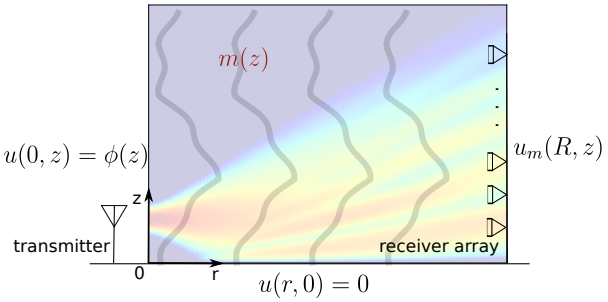

Fig. 1. Schematic of the bistatic configuration. Initial field $\phi(z)$ propagates rightward in horizontally stratified atmosphere, which is characterized with refractivity $m(z)$. Our goal is to retrieve $m(z)$ from wavefield measurements obtained with receiver array at distance R from the known source.

Our objective is to investigate the potential of MPT to mitigate the nonlinearity of the problem in our context, prior to curing the ill-posedness using regularization [6], [7]. In this work, we propose the recipe for multiscale least-squares inverse problem using adjoint state method for wide-angle parabolic equation. The novelty of this work is in the innovative solution proposed for the high-dimensional tomography problem discussed in [4], by tailoring the multiscaling idea in [7] and by fusing it with the method developed in [8], so as to build an improved refractivity inversion strategy which ideally works without the need for apriori information about the ambient conditions. We validate our strategy and show the improvement through the inversion of synthetic data. The problem is formulated in Section II and validation and inversion results are given in Section III.

II. Modeling

We study the problem of inferring the atmosphere from wavefield measurements obtained in the bistatic configuration

illustrated in Fig. 1, which is called the tomography problem in this paper. From a known source, initial field propagates towards a vertically-positioned receiver array in horizontally stratified atmosphere. The refracted propagating field is measured with this receiver array at several altitude points at a distance from the source. Our goal is to invert the refractivity of the atmosphere from the wavefield measurements obtained with receiver array, for given source and ground conditions. We invert synthetically-generated data because we do not have access to real-world measurements. In this section, we present the formulations defining this inverse problem and describe our solution strategy.

A. Standard Adjoint-based Tomography

We are interested in the estimation of the refractivity coefficient $m(z)$ of the wide-angle parabolic wave equation given below [9]:

$$\partial_r u + j\left[k_0(m(z)-1) + \left(\sqrt{k_0^2+\partial_z^2} - k_0\right)\right]u = 0, \quad \text{(1a)}$$

$$u(0,z) = \phi(z), \quad \text{(1b)}$$

$$u(r,0) = 0. \quad \text{(1c)}$$

In (1), the state function $u(r,z) \in \mathbb{C}$ is related to the electric or magnetic field propagating at frequency $f = k_0 c/2\pi$ through a medium with refractive index $m(z)$.

The refractivity function $m(z)$ is inferred from synthetically generated wavefield measurements taken vertically at a given distance R from the known source at all altitude points in domain $\Omega = [0,R]\times[0,Z]$ as given in Fig. 1. In this scenario, we assume that we do not have access to the phase of the complex function u during measurements. In this case, the inverse problem is formulated as the minimization of the square error functional over parameter m as given below:

$$\min_{m\in M_{\text{ad}}} J(m) = \frac{1}{2}\int_0^Z \left||u_m^{\text{sim}}(R,z)|^2 - d^{\text{obs}}\right|^2 dz. \quad (2)$$

In the cost function (2), d^{obs} is the synthetically generated measurement function in interval $z\in[0,Z]$ using m_{OBJ} such that $d^{\text{obs}} = |u^{\text{sim}}_{m_{\text{OBJ}}}(R,z)|^2$ by solving (1). The cost function is minimized using gradient-based optimization method (see [4] for a worked example). The gradient of the cost function $J(m)$ with respect to control parameter m is given below as proposed by [8]:

$$\nabla_m J = \Re\left\{ jk_0 \int_0^R w_m(r,z)\cdot\overline{u_m(r,z)}\; dr\right\}. \quad (3)$$

The function $w_m(r,z)\in\mathbb{C}$ is the adjoint function of the first order sensitivity of u with respect to m. It is the solution of the following equation as proposed by [8]:

$$\partial_r w_m + j\left[k_0(m-1) + \left(\sqrt{k_0^2+\partial_z^2} - k_0\right)\right]w_m = 0, \quad \text{(4a)}$$

$$w_m(R,z) = 2\left(|u_m(R,z)|^2 - d^{obs}\right)u_m(R,z), \quad \text{(4b)}$$

$$w_m(r,0) = 0. \quad \text{(4c)}$$

Solving (2) for high-dimensional m is a highly ill-posed problem even in the absence of modeling or measurement errors and noise [4]. In the next section, we explain how to apply the search space reduction technique to reduce the complexity of (2), referring the works in [6], [7].

B. Search Space Reduction

The motivation behind the search space reduction is to increase the efficiency of optimization. In the context of this study, search space reduction can be used for reducing the dimensionality of the problem so as to explore the search space in a well-organized economical fashion. Besides, the interest can be to restrict the search direction such that some non-physical local minima are avoided, or inversion parameters are polished (e.g. filtered, regularized) [6]. The reader is referred to [6] for further information about these ideas.

Subspace approaches are used for the investigation of search space reduction as described in [6]. For this study, a parameter model perturbation $\tilde{m}\in\mathbb{R}^{N_z}$ can be restricted to lie in an N_L-dimensional subspace of $\mathbb{R}^{N_z}$. This subspace is spanned by the vectors $\{a_i\}_{i=1,\dots,N_L}$, with $N_L < N_Z$. Then, $\tilde{m}$ is given by:

$$\tilde{m} = \sum_{i=1}^{N_L} q_i a_i = Aq. \quad (5)$$

Here, $q_i\in\mathbb{R}^{N_L}$ are the new parameters of inversion and $A = [a_1,\dots,a_{N_L}]\in\mathbb{R}^{N_z\times N_L}$ is the reduction basis [6].

In the context of RFC, subspace methods have typically looked for a good choice of reduction basis so that the atmosphere is resolved with an acceptable agreement to the observation. To achieve this, apriori knowledge about the atmosphere is required [10], [11]. However, our goal here is not to solve the entire of a particular type of problem with the best reduction basis. Instead, we look for a generic method to obtain a good starting point which represents the global structure of the atmosphere. This can be later used for retrieving a more detailed description of the atmosphere. Therefore, it is sufficient if our basis functions could capture roughly the global structure of the ambient refractive index at a given resolution level.

The gradient at this reduced resolution level can be computed efficiently by using (3). The gradient of the cost function $\tilde{J}(q)$ in this reduced space with respect to q can be inherited from the $\nabla_m J(m)$ in (3) using the chain rule:

$$\tilde{J}(q) := J(Aq) \;\text{ then }\; \nabla_q\tilde{J}(q) = A^T\,\nabla_m J(m). \quad (6)$$

The term $\nabla_q\tilde{J}(q)\in\mathbb{R}^{N_L}$ is called the reduced gradient at multiscale parametrization level L in this paper.

Since the reduced gradient is restricted as a function of the reduction basis, the inversion accuracy depends on the choice of the basis. In the next section, we introduce an optimization strategy to reduce the importance of finding the best reduction basis in order to represent the ambient refractive index, following the ideas in [7] about multiscale strategies.

C. Multiscale Strategy for Adjoint-based Tomography

Proper parametrization of the model $m(z)$ can drastically change the performance of inversion algorithm. However in practice, it is difficult to compare different parametrizations or reduction bases and select the best, without the use of apriori information about the atmosphere. Nevertheless, a multiscale approach can be used for weakening the dependence of the inversions on the reduction basis progressively. Additionally, such approaches can mitigate the nonlinearity of the inverse problem [7], [12].

Multiscaling with hierarchical refinement strategy in the admissible parameter space is employed in this work. Such strategy can use (6) to optimize efficiently i.e., starting from an initial guess, next scale inherits the inverted parameters at the previous scale as its initial guess. In the next sections, we explain how this is accomplished in an example scenario.

III. Numerical Analysis

In this section, we validate the proposed methodology and apply it to the inversion of synthetically generated data. More details on the simulation and the validation can be found in [13].

A. Computational Setup

The computational domain Ω_{N_r,N_z} has the dimensions $R = 10$ km and $Z = 150$ m. It is discretized with a uniform grid with numbers of discretizations $N_r = 101$ and $N_z = 151$. The initial condition $\phi(z)$ is given by the complex-point source positioned at $(r_s, z_s) = (-100\text{ m}, 25\text{ m})$ with width of 5 m and radiation frequency of $f_s = 2$ GHz at horizontal polarization.

Refractivity m is described via modified refractivity M given by $M(z) = (m(z) - 1) \times 10^6$. The objective and the initial modified refractivity parameters are denoted by M_{OBJ} and M_{IG} respectively in Fig. 3a . Refractivity does not vary with range. The finite dimensional refractivity parameter m of the simulations is computed at grid nodes, i.e., $m \in \mathbb{R}^{N_z}$. Consequently, we aim at inverting $N_z = 151$ refractivity parameters.

Reduced refractivity q is mapped to m using piecewise-linear basis function. Parameter q is equidistantly distributed in altitude and m is computed using linear interpolation on q.

The functions u_m and w_m in (1) and (4) are estimated numerically using split-step wavelet technique [14]. The field is apodized with the Hanning window for $z > Z$. The ground is modeled using local image method. So as to improve the accuracy of the numerical method, we have used the splitting scheme given below [14], [9]:

$$u|_{r+\Delta r,z} = e^{B/2}\mathcal{T}^{-1}\left\{\mathcal{P}\mathcal{T}\left\{e^{B/2}u|_{r,z}\right\}\right\}, \qquad (7)$$

where $B = \{-jk_0(m-1)\Delta r\}$ is the term accounting for the atmosphere, $\mathcal{T}$ is the wavelet transform operator with compression, $\mathcal{T}^{-1}$ is the inverse wavelet transform, and $\mathcal{P}$ is the operator modelling the free-space propagation in the wavelet domain. The adjoint field is computed using the same numerical method.

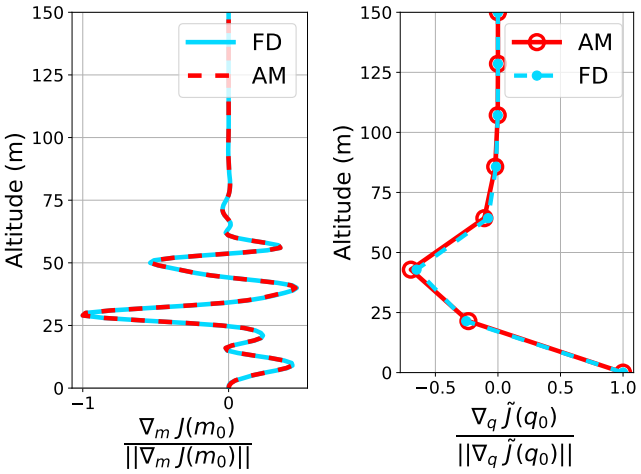

(a) Validation of gradient function (3).

(b) Validation of multiscale adjoint gradient function (6).

Fig. 2. Gradients estimated with the finite differences (FD) and the adjoint model (AM). The curves follow the synoptic structure of each other, so the multiscale adjoint method is validated.

The synthetic data is generated from function u by solving the forward model (1) for given objective parameter model m_{OBJ} using the split-step wavelet technique [14] with the splitting scheme (7). The numerical settings of the forward model used during inversions, as described earlier in this section, is the same as the one used during the synthetic data generation. Finite dimensional observation $d^{\text{obs}} = |u^{\text{sim}}_{m_{\text{OBJ}}}(R, z)|^2$ is sampled at each grid node in interval $z \in [0, Z]$ at range R, i.e., $d^{obs} \in \mathbb{R}^{N_z}$. The inversion aims at retrieving $M_{\text{OBJ}} \in \mathbb{R}^{N_z}$ by minimizing (2) iteratively using well-known BFGS algorithm [15], starting from an initial guess $M_{\text{IG}} \in \mathbb{R}^{N_z}$.

B. Validation of the Gradient

Since we use gradient-based optimization algorithm for solving (2), the inversion accuracy depends on how accurate the gradient is estimated. In this section, we validate the gradient functions (3) and (6). The validation is performed numerically using the baseline computational setup given in Section III-A.

In order to validate (3) and (4), the gradient function (3) which is estimated using Adjoint Model (AM), denoted by $\nabla_m J_{AM}$, is compared to the gradient function estimated using Finite Differences (FD), denoted by $\nabla_m J_{FD}$. Here, $\nabla_m J_{FD}$ is obtained using forward difference scheme for perturbation tolerance $\epsilon = 10^{-6}$. (Other values of ϵ have been tested. No significant dependence is observed.) The two gradients of the first iteration are computed as shown in Fig. 2a. The derived adjoint model is validated since it estimates the same gradient function computed by FD.

Next, we check if the reduced gradient is computed properly. To do so, we compute $\nabla_q \tilde{J}_{AM}$ using $\nabla_m J_{AM}$ with (6) for an arbitrary dimension of q, then plot it as shown in Fig. 2b. Next, we compute $\nabla_q \tilde{J}_{FD}$ by perturbing directly on q

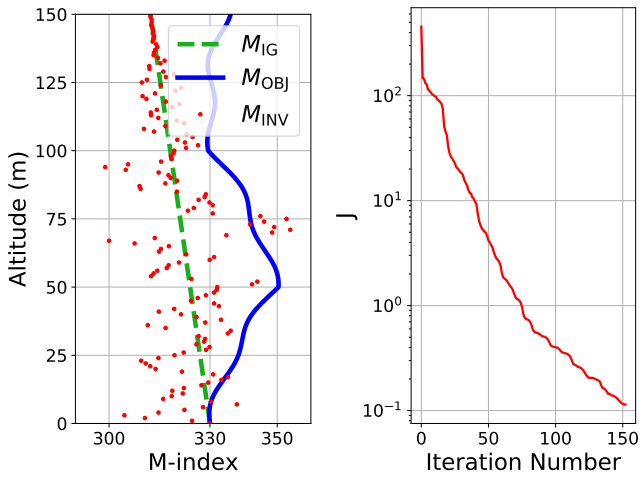

(a) Inversion without multiscaling.

(b) Convergence without multiscaling.

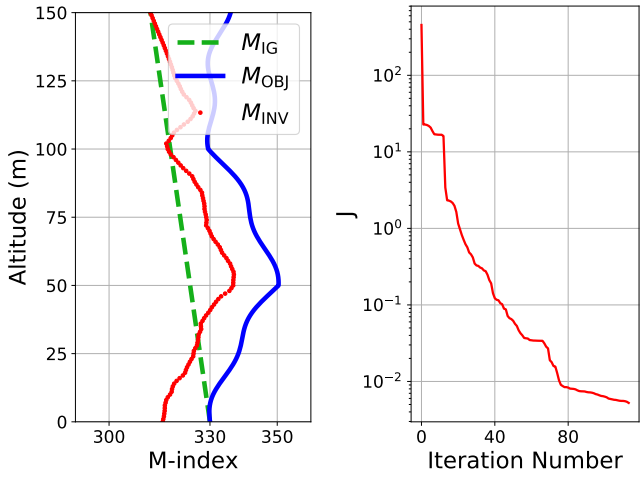

(c) Inversion with multiscaling.

(d) Convergence with multiscaling.

Fig. 3. Inverted parameters M_{INV} from synthetically generated data which corresponds to the same objective parameter M_{OBJ}, without multiscaling (i.e., using (3)) in 3a and with multiscaling (i.e., using (6)) in 3c and their convergence plots in 3b and 3d respectively. Inversion result improves with the use of multiscale parametrization.

using forward difference scheme. We observe an acceptable difference between FD and AM estimations, so the gradient of the multiscale approach is validated. The slight difference between FD and AM estimation in multiscale gradient validation probably comes from modeling error in $\nabla_m J_{AM}$. The splitting scheme (7) reduces this modelling error. In the next section, we show that the inversion result is improved using this reduced gradient in a multiscale strategy.

C. Preliminary Inversion Result

In this section, we explore the ability of our multiscale strategy to improve inversion results. To show the potential improvement, we select a baseline setup for which the gradient-based method fails to reach the global minimum without the use of multiscale strategy. Moreover, the objective parameter $M_{\text{OBJ}} \in \mathbb{R}^{N_z}$ is a complex profile such that it cannot be represented by any $q \in \mathbb{R}^{N_L}$ with $N_L < N_z$ considering the choice of our basis function. In other words, resolution of this ducting condition requires refinement of parameter at the finest level N_z.

In Fig. 3, we plot an inversion result together with the convergence, with and without multiscale strategy. With the choice of objective and initial guess parameters as in Fig. 3a, it is not possible to solve the problem accurately using only the plain adjoint-based method (i.e., the optimization is performed directly on the N_z dimensional search space M_{ad} using (3)). The result M_{INV} in Fig. 3a indicates the severity of nonlinearity and ill-posedness in the inverse problem. At this point, we assume that we do not have access to additional information to choose a good initial guess, pick the proper regularization strategy or the functional representation of m with few parameters, etc.

Multiscale strategy is now used for tackling this problem without additional apriori information. To show that in a numerical test, we perform 3 levels of multiscaling using the reduced gradient: we start with a 4-parameter inversion and refine the parameter dimension to 26 and 76 progressively. Then, we solve the 151-dimensional problem with the initial guess inherited from the inverted parameters of multiscale strategy. The obtained inversion result is as shown in Fig. 3c. The inversion is able to recover the general shape of the objective duct in many altitude points. By doing that, we achieve lower cost function compared to the case where multiscaling is not used (see Figs. 3b and 3d). The inversion result indicates that our multiscale strategy is suitable to cope with that level of inversion complexity at $R = 10$ km. In fact, since the global structure of the duct is approximated properly at the first level, the cost function decrease monotonically as the parameter dimension increases between the multiscale levels (see Fig. 3d). More testing is necessary to confirm the potential of the proposed methodology.

In practical applications, our altitude of interest to invert can be greater than the length of the receiver array. In order to test how the technique performs when the data is available only at the first few meters above the sea level, we limit the length of the receiver array to 30 m. Solving this inverse problem required imposing bounds on the optimization parameters since the optimization parameters diverged from the admissible parameter space with iterations. Therefore, a well-known L-BFGS-B algorithm [16] is used bounding the optimization parameters in the interval of $300-350$ M-unit at the sea level and in the interval of $280-380$ M-unit elsewhere. Inversion result of this scenario is presented in Fig. 4. Inversion retrieves roughly the gradient of objective refractivity M_{OBJ} only at the first few meters. Widening the interval of optimization bounds does not have prominent impact on the synoptic structure (gradient) of the inverted parameters at $z \in [0, 50]$ m, so the bounds values are chosen considering the presentability of the results in Fig. 4. More testing and validation is necessary to improve the potential of this methodology in dealing with lack

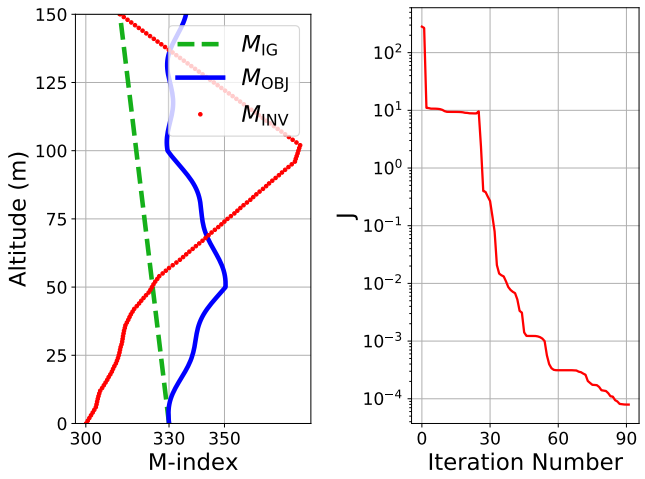

(a) Inversion. (b) Convergence.

Fig. 4. Inverted parameters M_{INV} using synthetically generated data from only the first 30 meters, with multiscaling (i.e., using (6)) and the convergence plot. Inversion retrieves roughly the gradient of objective refractivity M_{OBJ} only at the first few meters.

of measurement data.

IV. Conclusion

In this paper, we apply a multiscale parametrization to reduce the nonlinearity of refractivity inversion problem. We have shown that a proper hierarchical refinement strategy improves the inversion results. Our goal is to achieve unrealistically good inversion results on synthetic data, before inverting real world measurements. Note that we only used a basic linear interpolation for reducing the parameter vector dimension of the problem. A more proper choice of reduction basis can be found for accelerating the inversions and for reducing the sensitivity of inversions to the initial guess. Solving more complex ducting conditions (e.g., longer propagation ranges, more realistic ducts, noisy measurements) will be performed in a future study.

Acknowledgment

We would like to thank the anonymous referees for their comments which improved the presentation of the paper. This work is part of activities of ENAC/ISAE-SUPAERO/ONERA Research Federation.

References

[1] J. Krolik and J. Tabrikian, "Tropospheric refractivity estimation using radar clutter from the sea surface," in *Proceedings of the 1997 Battlespace Atmospherics Conference, SPAWAR Syst. Command Tech. Rep*, vol. 2989, 1998, pp. 635–642.

[2] R. Douvenot, V. Fabbro, P. Gerstoft, C. Bourlier, and J. Saillard, "A duct mapping method using least squares support vector machines," *Radio Science*, vol. 43, 2008.

[3] A. Karimian, C. Yardim, P. Gerstoft, W. S. Hodgkiss, and A. E. Barrios, "Refractivity estimation from sea clutter: An invited review," *Radio Science*, vol. 46, pp. 1–16, 2011.

[4] X.-F. Zhao, S.-X. Huang, and H.-D. Du, "Theoretical analysis and numerical experiments of variational adjoint approach for refractivity estimation," *Radio Science*, vol. 46, 2011.

[5] X. Zhao, C. Yardim, D. Wang, and B. M. Howe, "Estimating range-dependent evaporation duct height," *Journal of Atmospheric and Oceanic Technology*, vol. 34, no. 5, pp. 1113–1123, 2017.

[6] Y. Diouane, S. Gratton, X. Vasseur, L. N. Vicente, and H. Calandra, "A parallel evolution strategy for an earth imaging problem in geophysics," *Optimization and Engineering*, vol. 17, no. 1, pp. 3–26, 2016.

[7] C. Chavent and J. Liu, "Multiscale parametrization for the estimation of a diffusion coefficient in elliptic and parabolic problems," *IFAC Proceedings Volumes*, vol. 22, no. 4, pp. 193–202, 1989.

[8] U. Karabaş, Y. Diouane, and R. Douvenot, "A variational adjoint approach on wide-angle parabolic equation for refractivity inversion," *IEEE Transactions on Antennas and Propagation*, 2021, in press.

[9] F. B. Jensen, W. A. Kuperman, M. B. Porter, and H. Schmidt, *Computational Ocean Acoustics*. Springer Science & Business Media, 2011.

[10] P. Gerstoft, L. T. Rogers, J. L. Krolik, and W. S. Hodgkiss, "Inversion for refractivity parameters from radar sea clutter," *Radio Science*, vol. 38, no. 3, 2003.

[11] S. Kraut, R. H. Anderson, and J. L. Krolik, "A generalized Karhunen-Loeve basis for efficient estimation of tropospheric refractivity using radar clutter," *IEEE Transactions on Signal Processing*, vol. 52, no. 1, pp. 48–60, 2004.

[12] C. Bunks, F. M. Saleck, S. Zaleski, and G. Chavent, "Multiscale seismic waveform inversion," *Geophysics*, vol. 60, no. 5, pp. 1457–1473, 1995.

[13] U. Karabaş, Y. Diouane, and R. Douvenot, "On the use of adjoint methods for refractivity estimation in the troposphere," in *2020 14th European Conference on Antennas and Propagation (EuCAP)*. IEEE, 2020.

[14] H. Zhou, R. Douvenot, and A. Chabory, "Modeling the long-range wave propagation by a split-step wavelet method," *Journal of Computational Physics*, vol. 402, p. 109042, 2020.

[15] J. Nocedal and S. Wright, *Numerical Optimization*. Springer Science & Business Media, 2006.

[16] C. Zhu, R. H. Byrd, P. Lu, and J. Nocedal, "Algorithm 778: L-BFGS-B: Fortran subroutines for large-scale bound-constrained optimization," *ACM Transactions on Mathematical Software (TOMS)*, vol. 23, no. 4, pp. 550–560, 1997.